Large magnetotransport properties in mixed-dimensional heterostructures of 2D Dirac van der Waals materials

Rizwan Ur Rehman Sagar [a,**], Babar Shabbir [b,c,*], Syed Muhammad Hasnain [d], Nasir Mahmood [e], Muhammad Husnain Zeb [c], B.N. Shivananju [b,c], Taimur Ahmed [e], Irfan Qasim [f], Muhammad Imran Malik [g], Qasim Khan [c], Khurram Shehzad [h], Adnan Younis [i], Qiaoliang Bao [b,***], Min Zhang [a,****]

[a] *Tsinghua Shenzhen International Graduate School, Tsinghua University, Shenzhen, 518055, PR China*

[b] *Department of Materials Science and Engineering, ARC Centre of Excellence in Future Low-Energy Electronics Technologies (FLEET), Monash University, Clayton, Victoria, 3800, Australia*

[c] *Key Laboratory of Optoelectronic Devices and Systems of Ministry of Education and Guangdong Province, College of Electronic Science and Technology and College of Optoelectronics Engineering, Shenzhen University, Shenzhen University, Shenzhen, 518060, PR China*

[d] *Queensland Micro- and Nanotechnology Centre, Griffith University, Nathan, 4111, Brisbane, Australia*

[e] *School of Engineering, RMIT University, 124 La Trobe Street, 3001, Melbourne, Victoria, Australia*

[f] *Department of Physics, Riphah International University, Islamabad, 44000, Pakistan*

[g] *School of Electrical Engineering and Computer Science (SEECS) National University of Sciences and Technology (NUST) H-12, Islamabad 44000, Pakistan*

[h] *School of Information Science and Electronic Engineering, Zhejiang University, Hangzhou, 310027, PR China*

[i] *School of Materials Science and Engineering, University of New South Wales, Sydney, NSW, 2052, Australia*

ARTICLE INFO

ABSTRACT

Mixed dimensional van der Waals heterostructures (MD-vdWhs) open a huge potential to fabricate novel devices based on numerous metamaterials with superior magnetotransport properties. In conventional vdWhs, a variety of two dimensional (2D) layers has been stacked together to demonstrate vdWhs with phenomenal functionalities. However, creating 2D materials and their vdWhs over large areas with excellent magnetoresistance (MR) characteristics remains a major challenge. Graphene foam (GF), a 3D form of Dirac graphene continued to gather much attention for magnetotransport applications due to its large area/cost effective production and better magnetoresistance properties. Also, many combinations could be possible with GF to create numerous MD-vdWhs with hybrid functionalities, potentially giving access to explore novel devices with unique hybrid properties. Herein, we demonstrate MD-vdWhs (2D + 3D) of GF with molybdenum disulfide (MoS_2) to investigate magnetotransport properties. Remarkably, MR of GF is increased from ~130% to ~210% at 5 K under an applied magnetic field of 5 T by fabricating its MD-vdWhs with MoS_2. Our systematic investigations show that distinct magnetotransport properties in GF/MoS_2 vdWhs are strongly correlated to the enhancement in spin-orbit-coupling of the MD-vdWhs. Together, these results present a promising path toward the fabrication of future sensing and storage devices.

© 2020

1. Introduction

Synergetic materials based on vdWhs have recently been emerged with hybrid novel properties, paving the way for design of future technologies and particularly in devices with excellent magnetotrans-port functionalities [1–8]. The magnetotransport functionalities have been widely employed in many technologies specifically in magnetic sensing and storage devices, where the MR curve is a true figure of merit to define the device performance and/or efficiency. Generally, 2D + 2D vdWhs are utilized to precisely control the unique magnetotransport properties of hybrid materials at nanoscale. Even though 2D + 2D vd-Whs mostly consists of graphene seems very interesting in terms of fundamental science and potential applications. But, they have several disadvantages such as transfer & fabrication of 2D + 2D-vdWhs [9], lattice mismatch [10] and more importantly, the growth of single-crystal large area 2D materials are explicitly challenging to make devices for relevant measurements [11]. Perhaps, little progress has been made to synthesize polycrystalline 2D materials in centimeter scale, but granular structures play a significant role in degrading physical properties [12

* Corresponding author. Department of Materials Science and Engineering, ARC Centre of Excellence in Future Low-Energy Electronics Technologies (FLEET), Monash University, Clayton, Victoria, 3800, Australia.
** Corresponding author.
*** Corresponding authors.
**** Corresponding author.
E-mail addresses: rizwan.ts@sz.tsinghua.edu.cn (R.U. Rehman Sagar); babar.shabbir@monash.edu (B. Shabbir); qiaoliang.bao@monash.edu (Q. Bao); zhang.min@sz.tsinghua.edu.cn (M. Zhang).

] and therefore; device performances like those of single-crystal 2D + 2D-vdWhs could not be expected [11].

More recently, combinations of 2D + nD (n = 0, 1 and 3) materials or in other words known as MD-vdWhs i.e. 2D material integration to an array of materials with different dimensionalities; have started to emerge as an effective way to massively enhance critical properties in various fields [13,14] without damaging the structure which could be a case in other techniques such as pressure [15–19] and so on [20–22]. They can also be produced on a large scale with no requirement of lattice matching phenomena [23]. Therefore, investigation of magnetotransport mechanism in mixed dimensional vdWhs is highly desirable. Harnessing above mentioned factors, we opted GF as a target material to fabricate its MD-vdWhs based on the following reasons; GF is composed of monolayer, bilayers and multilayers graphene; commonly known as 3D architecture of dirac graphene because it incorporates the distinctive electrical properties of 2D graphene and thus it is highly conductive [24]. Also, many combinations could be possible with GF to create numerous MD-vdWhs with hybrid functionalities, potentially giving access to explore novel devices with unique hybrid properties.

Although, GF can easily be synthesized on a large scale and demonstrated linear positive MR of nearly 90% at 5 T and room temperature [25,26], however; because of weak SOC in graphene [27], enhancement of magnetotransport properties beyond a certain value is challenging. Theoretically, the problem of weak SOC in graphene could be completely addressed by creating its vdWhs with transition metal dichalcogenides [28]. Herein, we demonstrate MD-vdWhs (2D + 3D) of GF with MoS_2 to explore magnetotransport properties. Remarkably, MR of GF is increased from ~130% to ~210% at 5 K under an applied magnetic field of 5 T by fabricating its mixed dimensional heterostructures with MoS_2. Our systematic investigations show that obtained distinct magnetotransport properties in GF/MoS_2 vdWhs are strongly correlated to the enhancement in SOC of the MD-vdWhs hybrid system. Together, these results present a promising path toward strengthening of magneto transport properties in several materials and that can lead to develop unique sensing and storage devices with excellent efficiencies.

2. Results

To evaluate the morphology and formation of heterointerface, transmission electron microscopy (TEM) studies were carried out. The TEM image of the hybrid confirms the formation of GF/MoS_2 vdWhs with heterointerface in 2D fashion as shown in Fig. 1a-c. Moreover, to confirm the crystal structure of each component in the GF/MoS_2 vdWhs, HRTEM images were taken which clearly shows that presence of two different d-spacing values of 0.63 and 0.33 nm corresponds to MoS_2 according to JCPDS-37-1492 and graphene according to JCPDS-65-6212, respectively (Fig. 1c). Furthermore, the HRTEM image at the interface to construct the GF/MoS_2 MD-vdWhs in to of 3D framework confirms the presence of graphene and MoS_2 in a result of 3D designing (Fig. 1c). The selected area electron diffraction (SAED) pattern corresponds to six-fold Miller-Bravais indices, which are associated with the {1210}, {0110}, {1010} and {2110} atomic planes as shown in the inset of Fig. 1b, confirming the well-aligned growth and high crystallinity of the foam.

The crystalline structures of GF and its MD-vdWhs are analyzed by X-ray diffraction (XRD) and Raman spectroscopy, shown in Fig. 1d and e, respectively. The pure graphitic phase in GF is revealed by an obtained intense peak at $2\theta \approx 26.5°$ (standard card number: JCPDS-65-6212), which could be associated to (002) atomic plane (Fig. 1d). Two peaks are observed in GF/MoS_2-vdWhs at $2\theta \approx 26.5°$ and $2\theta \approx 14.4°$, which clearly indicates graphene and presence of MoS_2 (standard card number: JCPDS-37-1492), respectively. Also, few less intense peaks at $2\theta \approx 44.5°$ and $2\theta \approx 44.1°$ corresponds to graphene and MoS_2, as

shown in inset of Fig. 1d. Thus, GF and MoS_2 are both polycrystalline while GF/MoS_2-vdWhs contains both graphene and MoS_2 phases.

Fig. 1e displays a Raman spectra of a GF and its MD-vdWhs with prominent peaks namely D~1356 cm^{-1}, G~1581 cm^{-1} and 2D~2700 cm^{-1} are obtained for GF while another two peaks denoted as E_{2g}~380 cm^{-1} and A_{1g}~403 cm^{-1} are observed in GF/MoS_2 vdWhs. Obviously, the obtained E_{2g} and A_{1g} peaks and the space ($\Delta\omega$) between these bands, $\Delta\omega = (A_{1g} - E_{2g})$ in mixed dimensional vdWhs indicates MoS_2 [23]. The three specimens GF/MoS_2 (1, 3 and 5 min) with $\Delta\omega$~22 cm^{-1}, $\Delta\omega$~28 cm^{-1} and $\Delta\omega$~41 cm^{-1}, respectively demonstrates that the number of MoS_2 layers in MD-vdWhs depends on dipping times (Inset of Fig. 2e and also see Experimental Section for details). Furthermore, the ratios $A_{1g}/E_{2g} \sim 2.5$, $A_{1g}/E_{2g} \sim 2.7$ and $A_{1g}/E_{2g} \sim 3.2$ corresponds to GF/MoS_2 (1, 3 and 5 min) respectively, is another evidence to precisely control the number of MoS_2 layers by varying dipping times. The density of MD-vdWhs depend on the dipping time, where GF/MoS_2 -5 min indicates high densities and GF/MoS_2 -1 min shows low densities mixed vdWhs.

X-ray photoelectron spectroscopy (XPS) is carried out to analyze the surface chemistry of a material. Figs. S1(a–b) (supporting information) unveils two XPS peaks C1s and O1s in GF, where O1s is used as a reference peak to indicate peak shifting and the C1s peak shows no evidence of oxygen bonding, suggesting pure carbon bonding in GF. Further fitting of the peak with respect to C≡N exhibits its low intensity however, that could widen up for GF/MoS_2 specimen (Fig. 1g), possibly related to XPS chamber. The chemical state of surface atoms of GF/MoS_2-vdWhs shows the presence of S 2p$_3$, Mo 3d$_5$, C1s, Mo 3p$_3$ and O1s (Fig. 1f). The C1s spectra of GF/MoS_2-vdWhs is composed of a peak at ~284.4 eV, corresponded to C–C (Fig. 1g). The Mo 3d spectrum contain two doublets: Mo^{4+} 3d$_{5/2}$ = 229.04 eV & Mo^{4+} 3d$_{3/2}$ = 231.2 eV, and Mo^{6+} 3d$_{5/2}$ = 232.7eV & Mo^{6+} 3d$_{3/2}$ = 235.6 eV (Fig. 1h) [29]. The Mo^{4+} doublets are associated with the +4-oxidation state of Mo, while the Mo^{6+} state of MoO_3 emerges due to redox reactions. Furthermore, two peaks at binding energies ~161.9 and ~162.8 eV are associated to S 2p$_{3/2}$ and S 2p$_{1/2}$, respectively, a small shift might be due to formation of MD-vdWhs (Fig. 1i) [30,31]. These XPS peaks at particular binding energies can therefore, illustrates the formation of MD-vdWhs. This is further reflected in energy-dispersive spectroscopy analysis as shown in Fig. S1 of the Supporting Information. EDS-mapping of MD-vdWhs reveals the presence of carbon; red, sulfur; blue-green, and molybdenum; green as can be seen in i.e. Fig. S1d and its insets (Note: The surface topography of GF is shown in Fig. S1c). To evaluate MoS_2 contents in a GF, we have carried out the energy dispersive spectroscopy (EDS) analysis as presented in Figs. S1(e–h) of supporting information. Fig. S1h clearly shows the large contents of MoS_2 in GF/CZTS-5min as compared to the other GF specimens (Figs. S1e–g).

Utilizing four probe geometry (Fig. 2i), the magnetoresistance curves for GF and MD-vdWhs (1, 3 and 5mins) with material symbolic representation at different temperatures (in Kelvin or K) and magnetic fields (in Tesla or T) are shown in Fig. 2(a–h), respectively. At rather small fields (B < 2T), all MR curves generally tend to be quadratic, alike classical MR in semiconductors. However; MR becomes almost linear with fields greater than 2 T and that is in a good agreement with Abrikosov's conditions for quantum linear MR [32]. Overall, MR values in MD-vdWhs (1, 3 and 5mins) are found higher to that of GF. Take MD-vdWhs-5mins as an example, large values of around 210% are obtained at 5 K and 5T; nearly as twice as in GF i.e. ~130% (Fig. 2j). Similar enhancement trend at 5T is also noticed for other temperatures i.e., 50, 100, 200 & 300 K, and data is presented in Figure S2 (Supporting Information). Furthermore, MR curves for all specimens at different temperatures and 5 T is plotted in Fig. 2k. Even though, MR for MD-vdWhs-3 & 5mins can predict a roughly saturation regime in low temperatures but these data points are well above 100%; more impor-
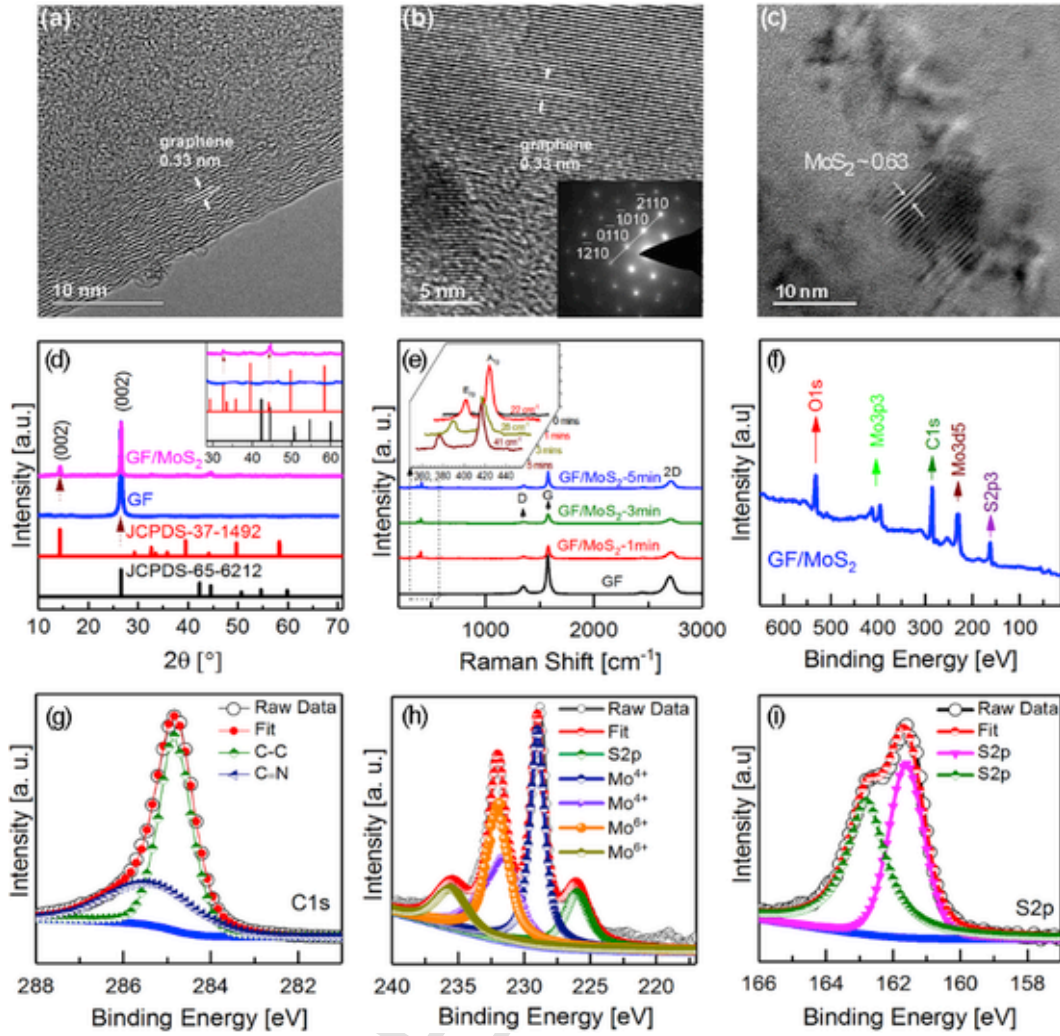
Fig. 1. Characterization of GF and GF/MoS₂-vdWhs. (a–b) HRTEM images of GF confirms few-layers to multilayer randomly oriented polycrystalline graphene and the inset in Figure b is the selected area electron diffraction (SAED) pattern shows different over lapping of different number of graphene layers with each other as indicates by the difference in the brightness of the dots. (c) HRTEM image of GF/MoS2-vdWh with a d-spacing ∼ 0.63 nm, indicating presence of MoS₂ (d) XRD pattern of GF; and GF/MoS₂-vdWhs contains both graphene and MoS₂ phases (e) Raman signatures of GF and GF/MoS2-vdWh (inset shows peaks A1g and E2g). The ratios $A_{1g}/E_{2g} \sim 2.5$, $A_{1g}/E_{2g} \sim 2.7$ and $A_{1g}/E_{2g} \sim 3.2$ corresponds to GF/MoS₂ (1, 3 and 5 min) respectively, illustrates an another evidence to precisely control the number of MoS₂ layers by varying dipping times. (f) X-ray photoelectron spectroscopy (XPS) is carried out to analyze the surface chemistry of a material. XPS survey is plotted for GF/MoS₂ (g), C1s (h), Mo3d (i) and S2p (i) spectra of GF/MoS₂-vdWhs. These XPS peaks at particular binding energies can therefore, illustrates the formation of mixed dimensional vdWhs. (A colour version of this figure can be viewed online.)

tantly at room temperatures and with linear responses. This is an ideal approach to build future magnetic sensors with linear and unsaturated responses that can work at room temperatures where no expenses are required to cool down the device for applications.

3. Discussion

To investigate large MR enhancement in GF/MoS₂ vdWhs materials; we have systematically examined different models. GF possess multiple conduction channels (Fig. 3a; schematic) due to different number of graphene layers present at each section. The fabrication of MD-vdWhs could also increase these conducting channels. The Hall resistance (R_{xy}) deviates from the linear dependence of the large magnetic field, indicates the multiple conducting channels like transport in GF (Fig. S3a of the SI) [33]. The resistance of the specimens decreases as the deposition time of MoS₂ increases (Fig. S3b of Supporting Information) and the total conductivity of GF can be expressed as

$$\sigma_{GF} = \sigma_1 + \sigma_2 + \sigma_3 + \sigma_4 \ldots \ldots \ldots \ldots \ldots .\sigma_n \tag{1}$$

where n is the number of graphene layers at different points during charge carrier transport. The charge carriers must selectively trans-

port through a particular conducting channel; for example, monolayer graphene is a zero band gap material, while bilayer graphene has a band gap of 0.25 eV [34] under an electrical field. In this regard, we can use a following probability equation

$$P(x) = \frac{n!}{(n-x)!\,x!} p^x q^{n-x} \tag{2}$$

in such a way that $P(x)$ is the probability of a charge carrier transporting through specific conducting channels (i.e., a specific graphene layer) within GF, n! counts the number of ways a charge carrier can travel from a specific conducting channel, $(n-x)!$ is the number of ways a charge carrier can pass through the same number of graphene layers, $x!$ excludes events when charge carrier passes through same number of graphene layers. p^x is the probability of the successfully transport charge carriers, and q^{n-x} shows unsuccessful transport of charge carriers. The mobility of GF specimens cannot be extracted experimentally as the thickness cannot be measured accurately due to nonuniform surface of graphene foam. However, we can utilize linear fitting of MR data to estimate mobility values (Fig. 3b). The mobil-
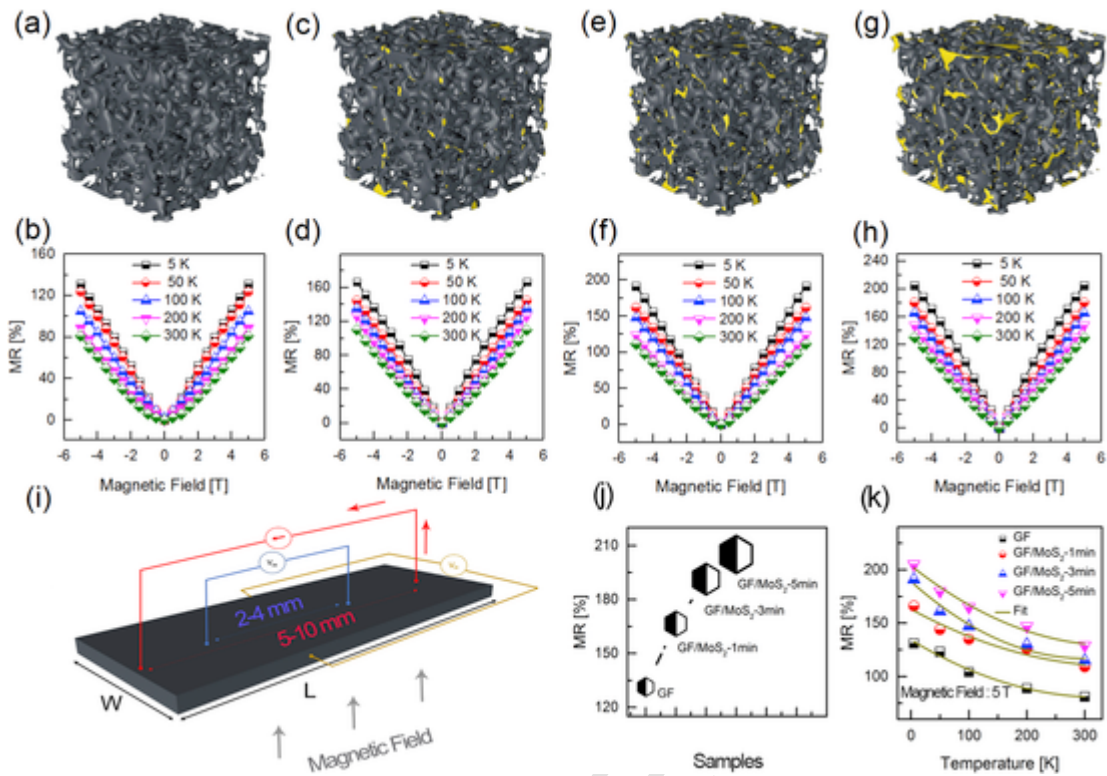
Fig. 2. Magnetotransport Properties of GF and GF/MoS₂-vdWhs. The schematic of (a) GF (c) GF/MoS₂-vdWhs-1min (e) GF/MoS₂-vdWhs-3mins (g) GF/MoS₂-vdWhs-5mins. The magnetoresistance data at different temperatures and fields are (b) GF (d) GF/MoS₂-vdWhs-1min (f) GF/MoS₂-vdWhs-3mins (h) GF/MoS₂-vdWhs-5mins. Magnetoresistance (%) magnitude is significantly enhanced in mixed dimensional vdWhs. At rather small fields, all magnetoresistance curves generally tend to be quadratic, alike classical magnetoresistance behavior in semiconductors. However; magnetoresistance becomes almost linear with fields greater than 2 T and that is in a good agreement with Abrikosov's conditions for quantum linear magnetoresistance [17] (i) Schematic of electric/magneto measurement unit. (j) MR (%) vs. different specimens at 5K and 5T. Take mixed dimensional VdWhs-5mins as an example, large values of around 210% are obtained at 5 K and 5T; nearly as twice as in graphene foam i.e. ~130% (j) MR (%) vs. temperature for different specimens at fixed magnetic field of 5 T. Even though, magnetoresistance for mixed dimensional vdWhs-3 & 5mins can predict a roughly saturation regime in low temperatures but these data points are well above 100%; more importantly at room temperatures and with linear responses. (A colour version of this figure can be viewed online.)
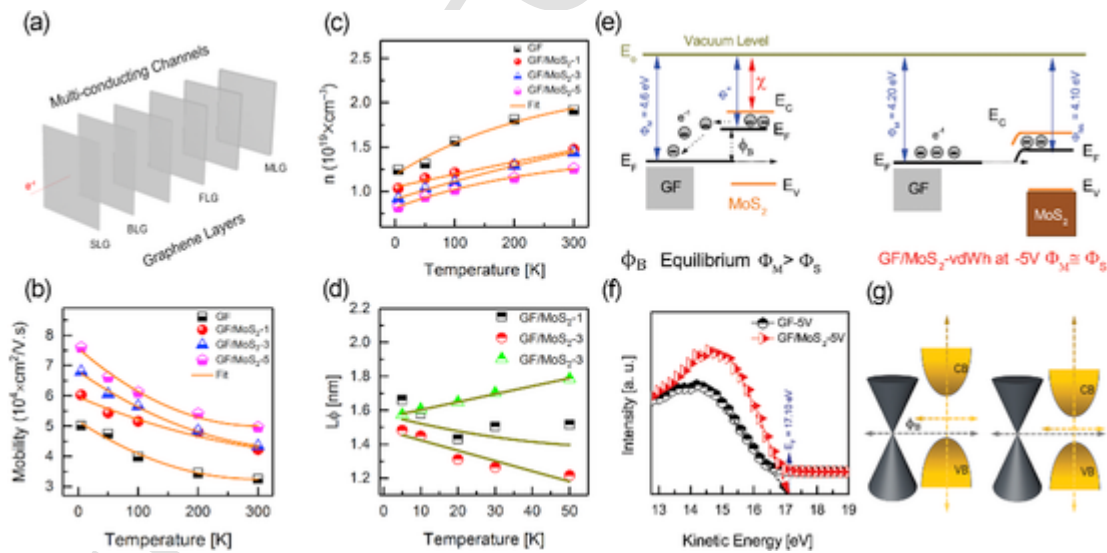

Fig. 3. Electronics of Charge Carriers: (a) Schematic of multi-conducting channels in graphene foam. (b) Mobility values at different temperatures for different specimens. The mobility of graphene foam specimens cannot be extracted experimentally as the thickness cannot be measured accurately due to nonuniform surface of graphene foam. Therefore, we have used linear fitting of MR data to estimate mobility values. The mobility (μ) of each specimen increases with the decrease in temperature, and the opposite is true for carrier density (*n*) plot (Fig. 3c). The *μ* of graphene foam is lower than those of all GF/MoS₂-vdWhs, indicating that MoS₂ may be deposited at low energy sites (i.e., defects), and thus, charge carriers were easily transported. (d) Phase coherence length vs. temperature for GF/MoS₂-vdWhs indicates an enhancement of spin orbit coupling in mixed dimensional vdWhs. (e) Band bending diagram of GF/MoS₂-vdWh under equilibrium and biased conditions (f) UPS of GF/MoS₂ under -5V in which graphene was positively charged (g) Rough representation for movement of the Fermi level in the equilibrium and biased conditions. (A colour version of this figure can be viewed online.)

ity (μ) of each specimen increases with the decrease in temperature, and the opposite is true for carrier density (n) plot (Fig. 3c) due to the freezing of a phonon-electron scattering. The μ of graphene foam is lower than those of all GF/MoS$_2$-vdWhs (Fig. 3b), indicating that MoS$_2$ may be deposited at low energy sites (i.e., defects), and thus, charge carriers were easily transported.

Tanabe et al. [35] reported electronic properties of GF and resistivity tensor according to semi-classical transport theory, as given below

$$\rho_{xx} = \rho_0 \mu B \frac{\tan^{-1}\mu B}{\left(\tan^{-1}\mu B\right)^2 + \left[\log(1+(\mu B)^2\right]^2/4} \tag{3}$$

in which μ is carrier mobility, B is applied uniform magnetic field, and $\omega_c\tau = \mu B$, ω_c is the cyclotron frequency and τ is the scattering time. According to semi-classical model, the large μ in GF/MoS$_2$ vdWhs (i.e. Fig. 3b) might explain the enhancement of positive MR in vdWhs specimens. On the other side; the quadratic MR behavior i.e. $MR \propto (\mu B)^2$, where $\mu = 5.5 \times 10^4 \text{cm}^2/\text{V.s}$ at room temperature for GF/MoS$_2$-5mins specimen which turns into~10^5% PMR at 5 T but in our case GF/MoS$_2$-5mins specimen shows 125% positive MR. Therefore, models depending on mobility are not useful to explain positive MR at high temperatures in GF.

GF is a hierarchical 3D framework of graphene and composed of graphene, bilayer and multilayers; therefore, the positive MR behavior in graphene foam specimens could be explained on the basis of graphene. The MR in multilayer graphene could be related to the weak localization and mathematically, written as [36].

$$\Delta\rho(B) \equiv \rho(B) - \rho(0)$$
$$= -\frac{(e\rho)^2}{\pi h}\left[F\left(\frac{B}{B_\phi}\right) - F\left(\frac{B}{B_\phi + 2B_i}\right) - 2F\left(\frac{B}{B_\phi + B_*}\right)\right] \tag{4}$$

Here $F(z) = \ln(z) + \psi\left(\frac{1}{2} + \frac{1}{z}\right)$, $B_{\phi,i,*} = \frac{hc}{4De}\tau_{\phi,i,*}^{-1}$, ψ−digamma function, D is a diffusion constant, h− plank's constant,$\rho(B)$ indicates resistivity as a function of magnetic field value. The correction to the sheet MR in eqn. (4); after including the isospin conserving scattering mechanism factor; can be expressed as [37].

$$\Delta\rho(B) \equiv -\frac{(e\rho)^2}{\pi h}\left[F\left(\frac{2\tau_\phi}{\tau_B}\right) - F\left(\frac{2}{\tau_B\left(\tau_\phi^{-1} + 2\tau_i^{-1}\right)}\right) - 2F\left(\frac{2}{\tau_B\left(\tau_\phi^{-1} + \tau_i^{-1} + \tau_w^{-1}\right)}\right)\right] \tag{5}$$

Here $\tau_\phi$is a phase coherence time, $\tau_i$denotes the intervalley scattering time, τ_w means the warping-induced relaxation time − linked to an intra-valley scattering due to the trigonal warping effect; $\tau_B = \hbar/2eDB$.

The weak or anti weak localization (WL, AWL) could be linked to the negative and positive linear MR in graphene [36,37]. The WL magnetoresistance generally depends on two types of scattering rates i.e. Elastic (chirality-breaking, τ_i, τ_w) and In-elastic (phase-breaking "τ_ϕ''"). The $F\left(\frac{2\tau_\phi}{\tau_B}\right)$ term in eqn (5) is linked to WL and $-F\left(\frac{2}{\tau_B\left(\tau_\phi^{-1}+2\tau_i^{-1}\right)}\right)$ and $-2F\left(\frac{2}{\tau_B\left(\tau_\phi^{-1}+\tau_i^{-1}+\tau_w^{-1}\right)}\right)$ terms are connected to AWL. The behavior of our positive MR data in GF therefore; shows WAL. Additionally, linear MR can be found in classical disorder systems is an another evidence [38]. The WAL in graphene can be strengthen further due to addition of a Rashba SOC as it attains an additional π phase in the

wave function [39]. As a matter of fact, the graphene has extremely weak intrinsic SOC but it can be enhanced by making its heterostructures with transition metal dichalcogenides (TMDs) [40]. The strong WAL presence in GF/MoS$_2$-vdWhs is another reflection of induced Rashba SOC. The large positive MR behavior in MD-vdWhs indicates the WAL effect, suggesting that GF acquires significant Rashba SOC due the formation of its MD-vDWhs with MoS$_2$. In mixed dimensional heterostructures materials, it is important to mention that the graphene dirac point is around a conduction-band minimum or the MoS$_2$ defect states [41]. This shows the enhancement of the band hybridization on the electron side. This could result in strongly asymmetric density of states and strong Rashba SOC due to stronger WAL.

Strong Rashba SOC in mixed dimensional heterostructures can be further evidenced by utilizing Hikami, Larkin, and Nagaoka (HLN) quantum interface model [42]. According to this model,

$$\Delta G(B) = -\frac{e^2}{2\pi h}\left[\psi\left(\frac{B_\varphi}{B}+\frac{1}{2}\right) - \ln\left(\frac{B_\varphi}{B}\right)\right]$$
$$-\frac{e^2}{\pi h}\left[\psi\left(\frac{B_{SO}+B_e}{B}+\frac{1}{2}\right)\right.$$
$$\left. - \ln\left(\frac{B_{SO}+B_e}{B}\right)\right]$$
$$+\frac{3e^2}{2\pi h}\left[\psi\left(\frac{\frac{4}{3}B_{SO}+B_\varphi}{B}+\frac{1}{2}\right)\right.$$
$$\left. - \ln\left(\frac{\frac{4}{3}B_{SO}+B_\varphi}{B}\right)\right] \tag{6}$$

in which, ψ is the digamma function, $e = 1.6 \times 10^{-19}$C is a the charge of an electron, and $h = 6.63 \times 10^{-34} m^2 Kg/s$ (Planck's constant), $B_i = \hbar/\left(4eL_i^2\right)$ is the characteristic field for the respective scattering mechanism ($i = \varphi, SO, e$), where L_φ is phase coherence length, L_{SO} is the spin-orbit scattering length, and L_e is the elastic scattering length. Assaf et al. [43] reported another approximation of the HLN model for a low magnetic field of less than 14 T, and the second term (spin-orbit scattering) and third term (elastic scattering), are approximated by a B^2-parabola as well as assuming that $L_\varphi \gg L_{SO}$. This approximation leads to

$$\Delta\sigma(B) = -\frac{\alpha e^2}{2\pi^2\hbar}\left(\ln\left(\frac{\hbar}{4el_\varphi^2 B}\right)\right.$$
$$\left. - \psi\left(\frac{1}{2}+\frac{\hbar}{4el_\varphi^2 B}\right)\right) + \beta B^2 \tag{7}$$

in which, α represents the number of conducting channels, and β is a quadratic coefficient. Eq. (7) is used to estimate L_φ for all specimens, and its magnitude is very small in comparison to the thickness of the specimen (Fig. 3d). Although, the L_φ decreases with increasing temperature in low densities MD-vDWhs i.e. GF/MoS$_2$-1 and GF/MoS$_2$-3 min specimens (Fig. 3d), but the increasing in L_φ in low temperature range for high densities mixed vdWhs i.e. GF/MoS$_2$-5 clearly indicates that enhanced spin orbit coupling is a main reason for the large enhancement of positive MR. The L_φ seems to be ineffective in high temperatures as plotted in Fig. S3d of supporting information, which is also true for SOC and further strengthen our argument. DFT calculations elsewhere also indicate the strong SOC in graphene heterostructures with different TMDs [41].

Here it is also worthy to mention that contact between a metal and a semiconductor can result in an ohmic or a Schottky junction depending upon the work function of both materials. In the GF/MoS$_2$-vdWh system, MoS$_2$ is a semiconductor and graphene is a metal. The work functions of pristine graphene and MoS$_2$ are 4.5 eV [44] and 5.3 eV [45], respectively. The work function of both materials depend on

the number of layers and a difference of 0.5–0.6 eV is observed for few-layer to multilayer materials. The difference in the work function of graphene and MoS_2, a difference of 0.7–0.8 eV, can produce a Schottky barrier during transport of charge carriers. Thus, Schottky junctions could be formed during the electrical transport, and these junctions can result in large magnetoresistance according to literature [46].

Albeit rough, the work function (Φ) of GF(Φ_M) and GF/MoS$_2$-vdWh(Φ_{MS}) are estimated under biasing by using the expression $\Phi = 21.2eV - (E_o - E_F)$, where E_o represents the cut-off binding energy, and E_F represents Fermi level. In the equilibrium condition, a barrier potential, φ_B, is formed due to discontinuity in the work functions of GF and MoS_2, which is reduced after the migration of charge carriers to graphene foam and therefore band bending starts and a built-in potential V_B appears. The results indicate that the work function of GF: $\Phi_M \sim 4.6 \pm 0.15$ eV under -5 V biasing conditions is in agreement with the literature [47]. The Schottky barrier $\varphi_B = e(\Phi_M - \chi)$, is a positive quantity ($\varphi_M > \chi$), when GF/MOS$_2$-vdWh comes in contact under the equilibrium condition. The Fermi levels of both materials start equilibrating due to the Schottky barrier, and some charge carriers do not have enough energy to cross φ_B. These charge carriers require extra energy which can be provided *via* biasing (Fig. 3e–g). Thus, both GF/MoS2-vdWh and GF are biased at -5 V, and the work function could be calculated. Φ_M is ~ 4.2, while Φ_{MS} is ~ 4.1, indicating that an ohmic junction was produced under the bias condition (Fig. 3f). Thus, the work function of GF/MoS$_2$ decreased after the application of a voltage, indicating that the Schottky barrier height decreased as well (Fig. 3g). The ohmic junction at room temperature is normally 25 meV of energy difference but herein, Schottky height ~ 100 eV is high enough to produce such a large change in the resistance of GF/MoS$_2$-vdWhs. However, Schottky barrier height reduces in biasing condition that indicates an easiness in the flow of charge carriers due to which the mobility of the charge carriers also enhanced in GF/MoS$_2$-vdWh-5 mins sample as shown in Fig. 3c. Thus, Schottky height could not clearly explained the large MR in GF/MoS$_2$-vdWhs.

4. Conclusions

We synthesized mixed-dimensional (2D + 3D) vdWhs of graphene foam with MoS_2 to investigate magnetotransport properties. The MR of GF is increased from $\sim 130\%$ to $\sim 210\%$ at 5 K under an applied magnetic field of 5 T by fabricating its MD-vDWhs with MoS_2. Systematic investigations are carried out to probe enhanced magnetotransport properties in GF/MoS$_2$ vdWhs systems and found that large and linear MR enhancement is strongly related to the enhancement in SOC of the MD-vDWhs system. Together, these results present a promising path toward strengthening of magneto transport properties in several materials and that can lead to develop unique sensing and storage devices with excellent efficiencies.

5. Experimental methods

5.1. Synthesis of graphene foam

Graphene foam was synthesized via chemical vapor deposition (CVD) method (Fig. S4a), as reported in the literature. The nickel foam with specifications 80 PPI (pores per inch) was locally purchased. PPI is calculated as an average across the surface of the uncompressed nickel foam. The pore density (uncompressed) is same in all dimensions as it is a reticulated foam and magnetoresistance values are dependent on PPI cross-section. (i) The nickel foam substrate (80 PPI) was placed at the center of a furnace tube (Fig. 1a). (ii) A vacuum was created in a furnace tube with the help of a rotary pump. (iii) Furnace tube was heated to 1100 °C at a rate of 5 °C/min under a combined flow of hydrogen and argon (Fig. 1b). (iv) Ethylene (C_2H_4) was mixed with the provided mixture of gases for a specific time. (v) C_2H_4 was turned off

to allow the furnace tube to cool down naturally and waited until it comes back to room temperature. (vi) The specimens were then collected from the furnace tube.

5.2. Transfer of graphene foam

Graphene that was fabricated on nickel-foam was then transferred as free-standing Graphene Foam. To remove nickel, graphene/nickel foam specimens were dipped in the solution of $FeCl_3.6H_2O$ (Fig. S4c). The nickel etching process could take from several hours to days depending upon the porosity of the nickel foam. After etching nickel, graphene foam started to float on the surface of solution, indicating that a successful reaction has been taken place. To remove remaining residues in specimens, the graphene foam was transferred in another solution of hydrochloric acid (HCl) and clean water for several hours. Finally, graphene foam was dried in an oven at 50~100 °C for few hours.

5.3. Formation of GF/MoS2-vdWhs

According to the literature, the chemical dip coating strategy was used to synthesize GF/MoS$_2$-vdWhs. A solution was synthesized by dissolving 100 mmol L^{-1} of $(NH_4)_2MoS_4$ in dimethylformamide (DMF), and as-grown graphene foam was dipped in the solution for a particular period of time (Fig. S4). Three specimens were prepared GF/MoS$_2$-1-S1, GF/MoS$_2$-3-S2, and GF/MoS$_2$-5-S3 for different dip coating times of 1, 3, and 5 min, respectively. These specimens were then placed in a furnace at 500 °C for an hour to remove the DMF residue from the specimens.

5.4. Characterization of GF/MoS2-vdWhs

High-resolution transmission electron microscopy (HRTEM-FEI-Technai G^2-F30) and Raman spectroscopy (Renishaw-HR800 equipped with 532 nm laser excitation source) have been employed for the structural study. The morphology and elemental mapping of graphene foam and its mixed dimensional vdWhs were carried out by scanning electron microscopy (SEM-Hitachi, SU-70). X-ray Diffraction (XRD- Rigaku D/max 2500, $\lambda = 1.5406$ Å) and X-ray photoelectron microscopy (XPS- MICROLAB350-Thermo Scientific, USA) have been utilized for phase identification and the confirmation of GF/MoS$_2$-vdWhs formation, respectively. A quantum design physical property measurement system (PPMS)-9 equipped with special homemade puck was used to conduct electronic transport measurements for all specimens (Schematic of electric/magneto measurement unit with details of channel length is shown in Fig. 2i). Specially designed homemade puck consists of four probes positioned in a straight line with channel lengths of 4 mm between the middle two probes and 10 mm between the end probes respectively. A continuous current is passed through the two end probes and the potential drop was calculated across the middle two probes. Magnetic field was applied perpendicular to all specimens. Current *vs.* voltage (IV) curves were observed under different temperatures and 0 field for the magnetotransport properties (Fig. S3c of Supporting Information (SI)). Using $MR(\%) = \left(\frac{R_{xx}(B)}{R_{xx}(0)} - 1\right) X 100$, Magnetoresistance data was calculated, where $R_{xx}(B)$ = resistance under an applied magnetic field (B) and $R_{xx}(0)$ = resistance under zero magnetic field. We used material dimensions $\sim 10 \times 5 \times 4$ mm^3 for magnetotransport measurements. Here it is important to mention that we used graphene foam in its original shape for magnetoresistance measurements instead of breaking it into micro flakes, where magnetoresistance results are slightly different.

Author's Contribution

R.U.R. and B.S. contributed equally to this work. R.U.R. has fabricated mixed-dimensional heterostructures of graphene foam & molybdenum sulfide. R.U.R conducted and plotted experimental results. R.U.R and B.S. analyzed the experimental results and co-wrote a manuscript with the help of N.M and M. H.Z. Q.B and M.Z supervised the project. All the other authors helped in revisions and data interpretation.

CRediT authorship contribution statement

Rizwan Ur Rehman Sagar: Conceptualization, Methodology, Software, Writing - original draft. **Babar Shabbir:** Conceptualization, Methodology, Software, Writing - original draft. **Syed Muhammad Hasnain:** Writing - review & editing. **Nasir Mahmood:** Data curation. **Muhammad Husnain Zeb:** Data curation. **Taimur Ahmed:** Writing - review & editing. **Irfan Qasim:** Writing - review & editing. **Muhammad Imran Malik:** Writing - review & editing. **Qasim Khan:** Writing - review & editing. **Khurram Shehzad:** Writing - review & editing. **Adnan Younis:** Writing - review & editing. **Qiaoliang Bao:** Supervision. **Min Zhang:** Supervision.

Declaration of competing interests

None.

Acknowledgements

Appendix A. Supplementary data

Supplementary data to this article can be found online at https://doi.org/10.1016/j.carbon.2020.01.001.

References

[1] K. Gopinadhan, Y.J. Shin, R. Jalil, T. Venkatesan, A.K. Geim, A.H.C. Neto, H. Yang, Extremely large magnetoresistance in few-layer graphene/boron–nitride heterostructures, Nat. Commun. 6 (2015) 8337.

[2] B. Shabbir, M. Nadeem, Z. Dai, M.S. Fuhrer, Q.-K. Xue, X. Wang, Q. Bao, Long range intrinsic ferromagnetism in two dimensional materials and dissipationless future technologies, Appl. Phys. Rev. 5 (4) (2018) 041105.

[3] M.H. Zeb, B. Shabbir, R.U.R. Sagar, N. Mahmood, K. Chen, I. Qasim, M.I. Malik, W. Yu, M.M. Hossain, Z. Dai, Q. Ou, M.A. Bhat, B.N. Shivananju, Y. Li, X. Tang, K. Qi, A. Younis, Q. Khan, Y. Zhang, Q. Bao, Superior magnetoresistance performance of hybrid graphene foam/metal sulfide nanocrystal devices, ACS Appl. Mater. Interfaces 11 (21) (2019) 19397–19403.

[4] R.U.R. Sagar, H.I.A. Qazi, M.H. Zeb, F.J. Stadler, B. Shabbir, X. Wang, M. Zhang, Tunable sign of magnetoresistance in graphene foam – ecoflex® composite for wearable magnetoelectronic devices, Mater. Lett. 253 (2019) 166–170.

[5] Z. Yue, I. Levchenko, S. Kumar, D. Seo, X. Wang, S. Dou, K. Ostrikov, Large networks of vertical multi-layer graphenes with morphology-tunable magnetoresistance, Nanoscale 5 (19) (2013) 9283–9288.

[6] X. Wang, Y. Du, S. Dou, C. Zhang, Room temperature giant and linear magnetoresistance in topological insulator Bi2Te3 nanosheets, Phys. Rev. Lett. 108 (26) (2012) 266806.

[7] Z.J. Yue, C.B. Zhu, S.X. Dou, X.L. Wang, Observation of field-induced polarization of valleys in p-type Sb2Te3 single crystals, Phys. Rev. B 86 (19) (2012) 195120.

[8] Z.J. Yue, X.L. Wang, S.X. Dou, Angular-dependences of giant in-plane and interlayer magnetoresistances in Bi2Te3 bulk single crystals, Appl. Phys. Lett. 101 (15) (2012) 152107.

[9] Y. Liu, S. Zhang, J. He, Z.M. Wang, Z. Liu, Recent progress in the fabrication, properties, and devices of heterostructures based on 2D materials, Nano-Micro Lett. 11 (1) (2019) 13.

[10] X. Li, M.-W. Lin, J. Lin, B. Huang, A.A. Puretzky, C. Ma, K. Wang, W. Zhou, S.T. Pantelides, M. Chi, I. Kravchenko, J. Fowlkes, C.M. Rouleau, D.B. Geohegan, K. Xiao, Two-dimensional GaSe/MoSe2 misfit bilayer heterojunctions by van der Waals epitaxy, Sci. Adv. 2 (4) (2016).

[11] K.S. Novoselov, V.I. Falko, L. Colombo, P.R. Gellert, M.G. Schwab, K. Kim, A roadmap for graphene, Nature 490 (7419) (2012) 192–200.

[12] J.-K. Huang, J. Pu, C.-L. Hsu, M.-H. Chiu, Z.-Y. Juang, Y.-H. Chang, W.-H. Chang, Y. Iwasa, T. Takenobu, L.-J. Li, Large-area synthesis of highly crystalline WSe2 monolayers and device applications, ACS Nano 8 (1) (2014) 923–930.

[13] D. Jariwala, T.J. Marks, M.C. Hersam, Mixed-dimensional van der Waals heterostructures, Nat. Mater. 16 (2016) 170.

[14] S. Aslam, R.U.R. Sagar, H. Kumar, G. Zhang, F. Nosheen, M. Namvari, N. Mahmood, M. Zhang, Y. Qiu, Mixed-dimensional heterostructures of hydrophobic/hydrophilic graphene foam for tunable hydrogen evolution reaction, Chemosphere (2019) 125607.

[15] B. Shabbir, H. Huang, C. Yao, Y. Ma, S. Dou, T.H. Johansen, H. Hosono, X. Wang, Evidence for superior current carrying capability of iron pnictide tapes under hydrostatic pressure, Phys. Rev. Mater. 1 (4) (2017) 044805.

[16] B. Shabbir, X. Wang, S.R. Ghorbani, C. Shekhar, S. Dou, O.N. Srivastava, Hydrostatic pressure: a very effective approach to significantly enhance critical current density in granular iron pnictide superconductors, Sci. Rep. 5 (2015) 8213.

[17] B. Shabbir, X. Wang, S.R. Ghorbani, A.F. Wang, S. Dou, X.H. Chen, Giant enhancement in critical current density, up to a hundredfold, in superconducting NaFe0.97Co0.03 as single crystals under hydrostatic pressure, Sci. Rep. 5 (2015) 10606.

[18] B. Shabbir, X. Wang, Y. Ma, S.X. Dou, S.S. Yan, L.M. Mei, Study of flux pinning mechanism under hydrostatic pressure in optimally doped (Ba,K)Fe2As2 single crystals, Sci. Rep. 6 (2016) 23044.

[19] B. Shabbir, X.L. Wang, S.R. Ghorbani, S.X. Dou, F. Xiang, Hydrostatic pressure induced transition from δT_c to $\delta\ell$ pinning mechanism in MgB2, Supercond. Sci. Technol. 28 (5) (2015) 055001.

[20] B. Shabbir, M.I. Malik, N.A. Khan, Effect on diamagnetism and phonon modes due to Mg and Be doping at Ca sites in Cu0.5Tl0.5Ba2Ca3−yMy-Cu4O12−δ(y = 0 and 1.5 for M = Mg, Be) high temperature superconductors, J. Supercond. Nov. Magnetism 24 (6) (2011) 1977–1983.

[21] B. Shabbir, A. Ullah, N. Hassan, M. Irfan, N.A. Khan, Suppression of superconductivity due to enhanced Co doping in Cu0.5Tl0.5Ba2Ca2Cu3−yCoyO10−δSuperconductors, J. Supercond. Nov. Magnetism 24 (5) (2011) 1521–1526.

[22] A. Younis, S.E. Shirsath, B. Shabbir, S. Li, Controllable dynamics of oxygen vacancies through extrinsic doping for superior catalytic activities, Nanoscale 10 (39) (2018) 18576–18585.

[23] X. Cao, Y. Shi, W. Shi, X. Rui, Q. Yan, J. Kong, H. Zhang, Preparation of MoS2-coated three-dimensional graphene networks for high-performance anode material in lithium-ion batteries, Small 9 (20) (2013) 3433–3438.

[24] Z. Chen, W. Ren, L. Gao, B. Liu, S. Pei, H.-M. Cheng, Three-dimensional flexible and conductive interconnected graphene networks grown by chemical vapour deposition, Nat. Mater. 10 (2011) 424.

[25] R.U.R. Sagar, M. Galluzzi, C. Wan, K. Shehzad, S.T. Navale, T. Anwar, R.S. Mane, H.G. Piao, A. Ali, F.J. Stadler, Large, linear, and tunable positive magnetoresistance of mechanically stable graphene foam-toward high-performance magnetic field sensors, ACS Appl. Mater. Interfaces 9 (2) (2017) 1891–1898.

[26] R.U. Rehman Sagar, K. Shehzad, A. Ali, F.J. Stadler, Q. Khan, J. Zhao, X. Wang, M. Zhang, Defect-induced, temperature-independent, tunable magnetoresistance of partially fluorinated graphene foam, Carbon 143 (2019) 179–188.

[27] S. Konschuh, M. Gmitra, J. Fabian, Tight-binding theory of the spin-orbit coupling in graphene, Phys. Rev. B 82 (24) (2010) 245412.

[28] H. Zhang, C. Lazo, S. Blügel, S. Heinze, Y. Mokrousov, Electrically tunable quantum anomalous Hall effect in graphene decorated by 5d transition-metal adatoms, Phys. Rev. Lett. 108 (5) (2012) 056802.

[29] Y.T. Ho, C.H. Ma, T.T. Luong, L.L. Wei, T.C. Yen, W.T. Hsu, W.H. Chang, Y.C. Chu, Y.Y. Tu, K.P. Pande, E.Y. Chang, Layered MoS2 grown on c -sapphire by pulsed laser deposition, Phys. Status Solidi Rapid Res. Lett. 9 (3) (2015) 187–191.

[30] X. Wang, J. Wang, X. Zhang, Q. Tian, M. Liu, N. Cai, Y. Xue, W. Chen, W. Li, F. Yu, Nitrogen-Doped Cu2S/MoS2 heterojunction nanorod arrays on copper foam for efficient hydrogen evolution reaction, ChemCatChem 11 (4) (2019) 1354–1361.

[31] Y. Peng, Z. Meng, C. Zhong, J. Lu, W. Yu, Z. Yang, Y. Qian, Hydrothermal synthesis of MoS2 and its pressure-related crystallization, J. Solid State Chem. 159 (1) (2001) 170–173.

[32] A.A. Abrikosov, Quantum magnetoresistance, Phys. Rev. B 58 (5) (1998) 2788–2794.

[33] Y. Jing, S. Huang, K. Zhang, J. Wu, Y. Guo, H. Peng, Z. Liu, H.Q. Xu, Weak antilocalization and electron-electron interaction in coupled multiple-channel transport in a Bi2Se3 thin film, Nanoscale 8 (4) (2016) 1879–1885.

[34] Y. Zhang, T.T. Tang, C. Girit, Z. Hao, M.C. Martin, A. Zettl, M.F. Crommie, Y.R. Shen, F. Wang, Direct observation of a widely tunable bandgap in bilayer graphene, Nature 459 (7248) (2009) 820–823.

[35] Y. Tanabe, Y. Ito, K. Sugawara, D. Hojo, M. Koshino, T. Fujita, T. Aida, X. Xu, K.K. Huynh, H. Shimotani, T. Adschiri, T. Takahashi, K. Tanigaki, H. Aoki, M. Chen, Electric properties of Dirac fermions captured into 3D nanoporous graphene networks, Adv. Mater. 28 (46) (2016) 10304–10310.

[36] E. McCann, K. Kechedzhi, V.I. Fal'ko, H. Suzuura, T. Ando, B.L. Altshuler, Weak-localization magnetoresistance and valley symmetry in graphene, Phys. Rev. Lett. 97 (14) (2006) 146805.

[37] X. Wu, X. Li, Z. Song, C. Berger, W.A. de Heer, Weak antilocalization in epitaxial graphene: evidence for chiral electrons, Phys. Rev. Lett. 98 (13) (2007) 136801.

[38] J.H. Lee, E.K. Lee, W.J. Joo, Y. Jang, B.S. Kim, J.Y. Lim, S.H. Choi, S.J. Ahn, J.R. Ahn, M.H. Park, C.W. Yang, B.L. Choi, S.W. Hwang, D. Whang, Wafer-scale growth of single-crystal monolayer graphene on reusable hydrogen-terminated germanium, Science 344 (6181) (2014) 286–289.

[39] E. McCann, V.I. Fal'ko, z\-z symmetry of spin-orbit coupling and weak localization in graphene, Phys. Rev. Lett. 108 (16) (2012) 166606.

[40] B. Yang, M. Lohmann, D. Barroso, I. Liao, Z. Lin, Y. Liu, L. Bartels, K. Watanabe, T. Taniguchi, J. Shi, Strong electron-hole symmetric Rashba spin-orbit coupling in graphene/monolayer transition metal dichalcogenide heterostructures, Phys. Rev. B 96 (4) (2017) 041409.

[41] A. Avsar, J.Y. Tan, T. Taychatanapat, J. Balakrishnan, G.K.W. Koon, Y. Yeo, J. Lahiri, A. Carvalho, A.S. Rodin, E.C.T. O'Farrell, G. Eda, A.H. Castro Neto, B. Özyilmaz, Spin–orbit proximity effect in graphene, Nat. Commun. 5 (2014) 4875.

[42] S. Hikami, A.I. Larkin, Y. Nagaoka, Spin-orbit interaction and magnetoresistance in the two dimensional random system, Prog. Theor. Phys. 63 (2) (1980) 707–710.

[43] B.A. Assaf, T. Cardinal, P. Wei, F. Katmis, J.S. Moodera, D. Heiman, Linear magnetoresistance in topological insulator thin films: quantum phase coherence effects at high temperatures, Appl. Phys. Lett. 102 (1) (2013) 012102.

[44] O. Leenaerts, B. Partoens, F.M. Peeters, A. Volodin, C.V. Haesendonck, The work function of few-layer graphene, J. Phys. Condens. Matter 29 (3) (2017) 035003.

[45] J.H. Kim, J. Lee, J.H. Kim, C.C. Hwang, C. Lee, J.Y. Park, Work function variation of MoS2 atomic layers grown with chemical vapor deposition: the effects of thickness and the adsorption of water/oxygen molecules, Appl. Phys. Lett. 106 (25) (2015) 251606.

[46] Y. Dezheng, W. Fangcong, R. Yang, Z. Yalu, P. Yong, Z. Shiming, X. Desheng, A large magnetoresistance effect in p–n junction devices by the space-charge effect, Adv. Funct. Mater. 23 (23) (2013) 2918–2923.

[47] S. Samaddar, J. Coraux, S.C. Martin, B. Grevin, H. Courtois, C.B. Winkelmann, Equal variations of the Fermi level and work function in graphene at the nanoscale, Nanoscale 8 (33) (2016) 15162–15166.